The ACE Magnetic Fields Experiment

Charles W. Smith, Jacques L'Heureux and Norman F. Ness
Bartol Research Institute, University of Delaware

Mario H. Acuña, Leonard F. Burlaga and John Scheifele
Code 695, NASA/Goddard Space Flight Center

(Received ..... ; Accepted in final form .....)

Abstract. The magnetic field experiment on ACE provides continuous measurements of the local magnetic field in the interplanetary medium. These measurements are essential in the interpretation of simultaneous ACE observations of energetic and thermal particles distributions. The experiment consists of a pair of twin, boom-mounted, triaxial fluxgate sensors which are located 165 inches (= 4.19 meters) from the center of the spacecraft on opposing solar panels. The electronics and digital processing unit (DPU) is mounted on the top deck of the spacecraft. The two triaxial sensors provide a balanced, fully redundant vector instrument and permit some enhanced assessment of the spacecraft's magnetic field. The instrument provides data for Browse and high-level products with between 3 and 6 vector s^{-1} resolution for continuous coverage of the interplanetary magnetic field. Two high-resolution snapshot buffers each hold 297 seconds of 24 vector s^{-1} data while on-board Fast Fourier Transforms extend the continuous data to 12 Hz resolution. Real-time observations with 1 second resolution are provided continuously to the Space Environmental Center (SEC) of the National Oceanographic and Atmospheric Association (NOAA) for near-instantaneous, world-wide dissemination in service to space weather studies. As has been our team's tradition, high instrument reliability is obtained by the use of fully redundant systems and extremely conservative designs. We plan studies of the interplanetary medium in support of the fundamental goals of the ACE mission and cooperative studies with other ACE investigators using the combined ACE dataset as well as other ISTP spacecraft involved in the general program of Sun–Earth Connections.

1. Introduction

The ACE Magnetic Field Experiment (MAG) will establish the time-varying, large-scale structure of the interplanetary magnetic field (IMF) near the L_1 point as derived from continuous measurement of the local field at the spacecraft. Measurements of the IMF will permit interpretation of particle distribution functions; determination of the source location for solar wind thermal and solar energetic particles through extrapolation of the local IMF; inference of the path taken by galactic cosmic rays in traversing the heliosphere; and analysis of the local source for *in situ* acceleration mechanisms. The MAG experiment will also measure the characteristics of the IMF fluctuations over a wide range of frequencies from the multi-year variability of the solar source to frequencies an order of magnitude greater than the proton gyrofre-

quency so that particle-scattering and transport dynamics can be better understood. The MAG experiment will establish the temporal variability of the large-scale structure of the IMF; MAG will correlate the IMF fluctuations with the large-scale variability; and MAG will serve future studies of the IMF turbulence that will in turn refine our understanding of cosmic ray propagation in the heliosphere.

This instrument will provide continuous measurements of the local IMF with 3 to 6 vector s^{-1} resolution for use in (1) automated, nonvalidated production of Browse data to provide quick-look values in support of preliminary scientific analyses and (2) timely production of best-quality data products for refined scientific analysis. In addition, snapshot memory buffer data and onboard Fast Fourier Transform (FFT) data based on 24 vectors s^{-1} will be provided as final data products. Both Browse and final data products will be available through the ACE Science Center [*Garrard and Hammond*, 1997]. The measurements will be precise (0.025%), accurate (± 0.1 nT), ultra-sensitive (0.008 nT/step quantization and 0.0005 nT/Hz in the most sensitive range), and have low noise with < 0.006 nT r.m.s. for 0 – 12 Hz. One vector s^{-1} values will be provided for real-time solar wind monitoring at a separate SEC/NOAA facility [*Zwickl et al.*, 1998].

The instrument configuration consists of a pair of boom-mounted, twin, triaxial fluxgate magnetometers with a shared DPU mounted on the top deck of the spacecraft. Each of the two sensors is mounted at the end of separate booms which are themselves mounted on the $+$Y and $-$Y solar panels [*Chiu et al.*, 1998]. Both triaxial sensors are located 165 inches = 4.19 meters from the center of the spacecraft with the sensor axes aligned with the axes of the spacecraft. The two sensor assemblies are identical and either can serve as the principal or sole sensor for the instrument. Deployment of the booms occurs shortly after instrument activation, approximately 1 hour after launch while the spacecraft is within the Earth's magnetosphere. The MAG instrument remains on throughout the mission, during the transit to L_1, and while the observatory is on station.

MAG is the reconditioned flight spare of the WIND Magnetic Field Investigation (MFI) [*Lepping et al.*, 1995]. Modifications were made to interface the instrument to the ACE data bus and to accommodate the reduced telemetry rate allocation provided for the instrument. The digital processing unit uses a 12-bit A/D converter that is microprocessor controlled to accurately resolve small amplitude fluctuations of the field. It also incorporates a dedicated FFT processor, developed around high-performance digital signal processor (DSP) integrated circuits, which produces a 32-channel logarithmic spectrum for each axis, synthesized from a 'raw' 256-point linear spectrum. All components of

the power spectral matrices corresponding to the 32 estimates are transmitted to the ground in 80 seconds providing both power and phase information. Each of the two snapshot memory buffers holds 5 minutes of high-resolution, 24 vector s^{-1} data and requires 5440 seconds (90.7 minutes) to download into spacecraft memory. Twin snapshot memory buffers permit one to be searching for a trigger event and recording high-resolution measurements while the other is downloading a captured event to spacecraft memory. As with other instruments of this heritage, high reliability is obtained by the use of fully redundant systems and extremely conservative designs. The intrinsic zero drift of the sensors is expected to be < 0.1 nT over periods of up to 6 months. Electrical 'flippers' designed to simulate a 180° mechanical rotation of the sensors will be used to monitor the zero-level drift associated with any possible aging of electronic components. The use of advanced statistical techniques for estimating absolute zero levels, including spacecraft fields, is also planned. The instrument features a very wide range of measurement capability, from ± 4 nT up to $\pm 65,536$ nT per axis in eight discrete ranges. The upper range permits complete testing in the Earth's magnetic field. Automatic switching between the ranges is a capability of the instrument as is range setting by command.

In the following section we describe some of the science we plan to pursue with the MAG instrument in cooperation with the ACE science team. Following that, we describe the MAG instrument in detail and conclude by describing the various data products that the MAG instrument team will deliver to the ACE Science Center for dissemination and use by the ACE team and the space physics community.

2. Scientific Objectives of the MAG Investigation

The ACE mission is first an investigation of the composition and abundances of energetic particles in near-Earth orbit. Following this, there is a great opportunity to use the ACE observations to study the propagation and evolution of thermal and energetic particle populations so that their characteristics at their respective sources and the dynamics of their origins and transport is better understood. The particles observed by ACE will have origins that range from the sun, through interplanetary space and planetary magnetospheres, to the interstellar medium and other stars of our galaxy. The particle populations are accelerated by a variety of source dynamics including coronal heating, wave resonances, magnetic reconnection, first and second order Fermi acceleration, drift acceleration and, in the case of pickup ions, photoionization and charge exchange. The particle populations evolve

significantly between the source location and the measurement and are modified in the interplanetary medium by many of the same general processes: wave resonances, magnetic reconnection (in the case of magnetospheric leakage events), first and second order Fermi acceleration, shock processing, and particle drift. It will be the task of ACE to measure charged particle populations at 1 AU and attempt to gain a better understanding of the source location and dynamics at these remote sites.

ACE is designed to study thermal and energetic particle populations including galactic cosmic rays, the anomalous component of cosmic radiation, interstellar pickup ions, solar cosmic rays, energetic storm particles, and particles originating at or behind the Earth's and Jupiter's bow shocks. In virtually every instance, with the possible exception of pickup ions, charged particles observed at L_1 originate at remote locations such as the sun or interstellar space. (Pickup ions are formed from interstellar neutrals that are locally ionized within the interplanetary medium.) In no instance are these particles observed with their original source distribution. All of the above distributions are processed in some manner by interaction with the solar wind as they stream from their source location (the interstellar medium, the sun, the Earth's bow shock, the Jovian magnetosphere, or the early formation region of interplanetary transients) to the point of observation. The magnetic field provides the coupling between the thermal and energetic charged particle distributions and the large-scale gradients of the solar wind. For this reason, detailed knowledge of the IMF and its fluctuations is necessary in order to understand how the interplanetary medium processes the particle distributions.

Energetic charged particles interact with the solar wind through the influence of the IMF. The magnetic field of interplanetary space is supported by the collective behavior of the charged particles that form the solar wind and interplanetary plasma. In a collisionless plasma, such as the solar wind, individual particle collisions are rare, but 'collisions' with the ambient magnetic field are continuous. When energetic charged particles encounter a large-scale (nearly global) disturbance which, either through a redirection of the IMF or through enhanced scattering by elevated turbulence levels, redirects the velocity of the energetic particles, these large-scale disturbances alter the particle distributions over a scale that is larger than the size of the disturbance. Likewise, particles interact with the ambient, undisturbed interplanetary medium in a continuous, diffusive manner due to the presence of low-level fluctuations, or turbulence. In this way, energetic particles such as cosmic rays interact with thermal particle populations via the ambient magnetic field in a self-consistent and deterministic manner.

The spatial and temporal scales that characterize the interplanetary magnetic field span the widest possible range and every scale affects the scattering, modulation and evolution of charged particle distributions. At the very largest scales, the *Parker* [1963] spiral and reversals of the spiral field associated with solar magnetic dipole reversals define the paths taken by galactic cosmic rays entering the heliosphere. Long-term solar variability (solar magnetic dipole reversals, multi-year trends in the solar activity cycle, etc.) as well as short-term (stream structures, the eruption of solar fields with different magnetic polarity, etc.) and individual transients (interplanetary shocks, coronal mass ejections (CMEs), etc.) alter these pathways and modulate the streaming of cosmic rays to varying degrees. Over the anticipated lifetime of the ACE spacecraft, the MAG instrument will record:

1. The Parker spiral field with continuous variations due to solar wind speed,
2. At least one solar magnetic dipole reversal in approximately the year 2003,
3. The emergence of sunspots and regions of opposing magnetic polarity leading to a complex structure of multiple interplanetary current sheets,
4. The passage of numerous and assorted transient structures including CMEs and interplanetary shocks,
5. Many stream interface regions,
6. Many heliospheric current sheet crossings,
7. Many recurrent interaction regions which may lead to shock pairs at greater heliocentric distance,
8. And periods of nearly radial IMF when the spacecraft is magnetically connected to the Earth's bow shock.

All of these observable features and processes define the magnetic field of the interplanetary medium, modify the particle distributions observed at L_1, and alter the evolution of the charged particle populations that are ultimately observed by the ACE spacecraft. By combining observations at L_1 with theoretical models for the evolution of the solar wind, we can extend the measurements beyond the observation point, sunward, and into the outer heliosphere.

The solar magnetic dipole and associated Parker spiral define the magnetic polarity and long-term global structure of interplanetary space,

and thereby control the diffusion and drift of galactic and anomalous cosmic rays toward the inner heliosphere [*Jokipii et al.*, 1977]. Reversal of the solar magnetic dipole reverses the direction of particle drift, which leads to an 11-year cycle in the galactic cosmic ray intensity at 1 AU. Recent observations by the Ulysses spacecraft of cosmic ray intensities over the solar poles that are lower than predicted by drift theory [*Simpson et al.*, 1995a,b] have brought into question the role of particle drifts in galactic cosmic ray propagation. New ACE observations, in coordination with a continued Ulysses mission, may reveal new insights into this problem so long as detailed magnetic field measurements are available at both locations.

A frequent feature of the inner heliospheric solar wind is the regular and periodic observation of recurrent interaction regions which form at the leading edge of corotating streams. Between 1 and 15 AU forward and reverse shock pairs form and corotating interaction regions (CIRs) merge to form corotating merged interaction regions (CMIRs) [*Burlaga et al.*, 1983; 1993]. Interactions among CMIRs, transient ejecta, and shocks occasionally form the global merged interaction regions (GMIRs) in the outer heliosphere that have a significant influence on the solar cycle-dependent transport of galactic cosmic rays. By making extended measurements of the IMF at 1 AU, it is possible to model the evolution of the interaction regions and compare these results with the time-dependent measurements of cosmic rays at 1 AU which originate from outside the heliosphere.

The large-scale magnetic field, as defined by whatever spatial scales are sampled by a particle of given energy over several gyroperiods, defines the average magnetic field followed by a particle as it moves through the heliosphere. Fluctuations of the IMF relative to that average are generally regarded to be sources for scattering the particle to other pitch angles or other field lines. At near-Earth orbit, the IMF is nominally oriented at 45° to the radial (sun-Earth) direction, but extended instances of nearly radial IMF and periods of nearly azimuthal fields are not uncommon. On average, the large-scale IMF at L_1 is nearly confined to the solar equatorial plane, but individual measurements almost always reveal a significant departure from this prediction that lasts for several hours. Averages over longer timescales are more nearly zero, but persistent, small, non-zero multi-year averages are seen and remain unexplained [*Smith and Bieber*, 1993; *Smith and Phillips*, 1997]. Any attempt to trace interplanetary observations of solar cosmic rays to the source on the sun must take into account the geometry of the large-scale field between 1 AU and the sun. That geometry can only be inferred, approximately, after observing the local field and solar wind

for days and attempting to reconstruct the IMF of the inner heliosphere over that time.

Additional transient phenomenon, such as CMEs and interplanetary shocks, can both alter the large-scale field and serve as a source of acceleration or scattering centers for particles streaming along the local IMF. CMEs represent additional and identifiable sources of solar wind particles with unique characteristics unlike the 'open' field lines neighboring it. Examination of the geometry of CME field lines helps to determine the source dynamics at the point where the CME originates and may shed some light on the associated process of particle energization that appears to take place in association with plasmoid ejection. The magnetic fluctuations within the CME can process the energetic and thermal particles contained within it while the closed field geometry of CMEs and magnetic clouds [*Burlaga*, 1995] acts as a barrier to external particles that would penetrate its surface and dilute the native particle population internal to the disturbance. In this way, CME thermal particles remain a distinct sample of the solar plasma with different parameters than the normal solar wind. Examination of this separate population, together with an improved understanding of the expansion and evolution of the magnetically contained plasma, should shed new insights into near-sun processes such as magnetic reconnection and some solar wind acceleration processes.

CME propagation through the interplanetary medium frequently produces shocks in the upstream region. Interplanetary shocks due to CMEs and other sources accelerate both thermal and suprathermal particles from the solar wind to form energetic storm particles upstream and downstream of the disturbance [*Forman and Drury*, 1983; *Lee*, 1984; *Sanderson et al.*, 1985] and as such process the *in situ* interplanetary particles in a manner that is both charge- and species-dependent. While significant strides have been made in understanding the acceleration processes, the initial injection mechanism for thermal particles remains a source of many questions. The scale of CME and interplanetary shocks is approximately 1 AU at near-Earth orbit, but the spatial scale of the boundary of these disturbances where significant interaction with the ambient particle population occurs can be as small as a few gyroradii of a thermal ion. By themselves, transient phenomena span both the largest and the smallest spatial scales in the solar wind.

While the ambient IMF fluctuations scatter charged particle populations, the exact nature of the IMF fluctuations remains a source of many questions and controversies. There is abundant evidence that the solar wind forms a turbulent magnetofluid that evolves in a nonlinear fashion from the source to its termination at $\sim$ 100 AU [*Coleman*, 1968; *Matthaeus and Goldstein*, 1982; *Roberts et al.*, 1987; *Tu and Marsch*,

1995; *Zank et al.*, 1996]. A component of that turbulence is outward-propagating Alfvén waves, which are particularly evident within the trailing regions behind high-speed streams [*Belcher and Davis*, 1971]. The theory of charged particle scattering by Alfvén waves is now well-developed [*Hasselmann and Wibberenz*, 1968]. However, there is growing evidence that $\sim 80\%$ of the magnetic fluctuation energy is carried by two-dimensional (2-D) turbulence that is self-organized and oriented at right angles relative to the large-scale magnetic field [*Matthaeus et al.*, 1990; *Zank and Matthaeus*, 1992; *Bieber et al.*, 1996] and there is some evidence that interaction between 2-D turbulence and thermal particles is significant [*Ambrosiano et al.*, 1988]. Preliminary analyses show that such 2-D fluctuations show very little interaction with energetic particles in the quasilinear limit [*Bieber et al.*, 1994], but quite compelling evidence exists that even a small percentage of 2-D turbulence can lead to a significant degree of field line diffusion [*Matthaeus et al.*, 1995; *Gray et al.*, 1996] which, in turn, leads to energetic charged particle diffusion. Consideration of such 2-D fluctuations have brought quasilinear theory into agreement with observed cosmic ray mean-free-paths while magnetodynamic revisions of the familiar magnetostatic quasilinear theory coupled to consideration of the smallest scale fluctuations that form the dissipation range of IMF turbulence has proven successful in accounting for the observed charge-dependent scattering rates of protons and electrons [*Bieber et al.*, 1994].

The MAG investigation will continue to study these and other interplanetary processes that have a direct effect on the evolution of thermal and energetic charged particle distributions. It is neither practical nor possible to list all such investigations, but this much is clear: Past efforts to advance the theory of cosmic ray propagation did not always anticipate the discoveries made by researchers in the field of solar wind research working on the theory and observations of the interplanetary magnetic field. Future studies of the heliospheric plasma will undoubtedly yield new insights into the nature of solar wind turbulence and the multi-spacecraft studies combining ACE with ISTP missions will be at the heart of many of these efforts. If past efforts are any indication, it is reasonable to expect that these new discoveries will have significant effects on our understanding of charged particle propagation in the heliosphere and will alter our view of cosmic ray physics. For this reason, the MAG investigation will continue to study the solar wind and IMF in the hope of uncovering new results of direct applicability to the fundamental mission of ACE.

3. MAG Instrument Description

The ACE MAG instrument is the reconditioned flight spare of the WIND/MFI experiment [*Lepping et al.*, 1995]. The only changes made to the unit were to accommodate the ACE data bus (the MFI I/O board was replaced) and to change the sampling rate of the instrument so that it better met the telemetry allocation for ACE (down from 44 vector s^{-1} for WIND to 24 vector s^{-1} for ACE). The WIND/MFI and ACE/MAG instruments are based on the magnetometers previously developed for the Voyager, ISPM, GIOTTO, Mars Observer, and Mars Global Surveyer missions which represent state-of-the-art instruments with unparalleled performance. Table I summarizes the principal characteristics of this instrument. The basic configuration consists of twin, wide-range (± 0.001 to $\pm 65{,}536$ nT) triaxial fluxgate magnetometers mounted on two deployable, titanium booms, a 12-bit resolution A/D converter system and a microprocessor controlled data processing and control unit (DPU). Both magnetometer sensors are deployed 165 inches (= 4.19 meters) from the center of the spacecraft along the $\pm$Y axes of the spacecraft.

There was no magnetics requirement for the ACE spacecraft, but an informal processes of screening and design review was maintained by the Johns Hopkins Applied Physics Laboratory (APL) and individual experimenters [*Chiu et al.*, 1998]. Screening of AC and static magnetic field characteristics of spacecraft components (both instruments and subsystems) was performed by members of the MAG team in cooperation with instrument and spacecraft system engineers throughout the spacecraft assembly process. Compensation of one subsystem unit was necessary in order to correct a large static field. Spacecraft-level testing of AC magnetic field characteristics was performed by MAG team personnel at APL prior to shipment of the observatory. No significant signals were detected. A simple mapping of the spacecraft's static field was performed at the Goddard Space Flight Center (GSFC) shortly after delivery of the observatory for environmental testing using portable magnetometers while the observatory was suspended from a crane. The static magnetic field of the ACE observatory prior to launch is estimated to be < 0.35 nT for each component at the deployed position of the MAG sensors. This value for the spacecraft field is too small to force a range change in the instrument and can easily be removed from the measurements by means of familiar data analysis methods that are designed to detect slowly changing instrumental offsets.

A block diagram of the MAG instrumentation is shown in Figure 1. The twin magnetometer system is supported by the fully redundant DPU which interfaces with the spacecraft data and power systems.

Table I. Summary of instrument characteristics

Instrument type:	Twin, triaxial fluxgate magnetometers (boom mounted)
Dynamic ranges (8):	$\pm$4 nT (Range 0); $\pm$16 nT (Range 1); $\pm$64 nT (Range 2); $\pm$256 nT (Range 3); $\pm$1024 nT (Range 4); $\pm$4096 nT (Range 5); $\pm$16,384 nT (Range 6); $\pm$65,536 nT (Range 7)
Digital Resolution (12-bit):	$\pm$0.001 nT (Range 0); $\pm$0.004 nT (Range 1); $\pm$0.016 nT (Range 2); $\pm$0.0625 nT (Range 3); $\pm$0.25 nT (Range 4); $\pm$1.0 nT (Range 5); $\pm$4.0 nT (Range 6); $\pm$16.0 nT (Range 7)
Bandwidth:	12 Hz
Sensor noise level:	$<$ 0.006 nT RMS, 0-10 Hz
Sampling rate:	24 vector samples/s in snapshot memory and 3, 4 or 6 vector samples/s continuous data stream
Signal Processing:	FFT Processor, 32 logarithmically spaced channels, 0 to 12 Hz. Full spectral matrices generated every 80 seconds for four time series (B_x, B_y, B_z, $\|B\|$)
FFT Windows/Filters:	Full despin of spin plane components, 10% cosine taper, Hanning window, first difference filter
FFT Dynamic range:	72 dB, μ-Law log-compressed, 13-bit normalized to 7-bit with sign
Sensitivity threshold:	$\sim 0.5 \times 10^{-3}$ nT/Hz in Range 0
Snapshot memory capacity:	256 Kbits
Trigger modes (3):	Overall Magnitude Ratio, Directional max.-min. peak-to-peak change, Spectral increase across frequency band (RMS)
Telemetry Modes:	Three, selectable by command
Mass:	Sensors (2): 450 g. total Electronics (redundant): 2100 g. total
Power Consumption:	2.4 watts, electronics - regulated 28 Volts $\pm$ 2% 1.0 watts, heaters - unregulated 28 Volts

The use of full redundancy in the MAG instrument is an important feature that emphasizes the critical nature of the magnetic field measurements for integrating the ACE observations into a consistent and cohesive interpretation of particle dynamics in the solar wind and for the achievement of the overall ACE science goals. Moreover, the fact that MAG is a fully redundant instrument, combined with the low mass, low power and low cost of the instrument, emphasizes the advanced state of development for this experiment. Electronic redundancy significantly reduces the probability of failures and takes advantage of the inherent redundancy provided by the twin magnetometer sensor configuration. This redundancy includes assigning by ground command

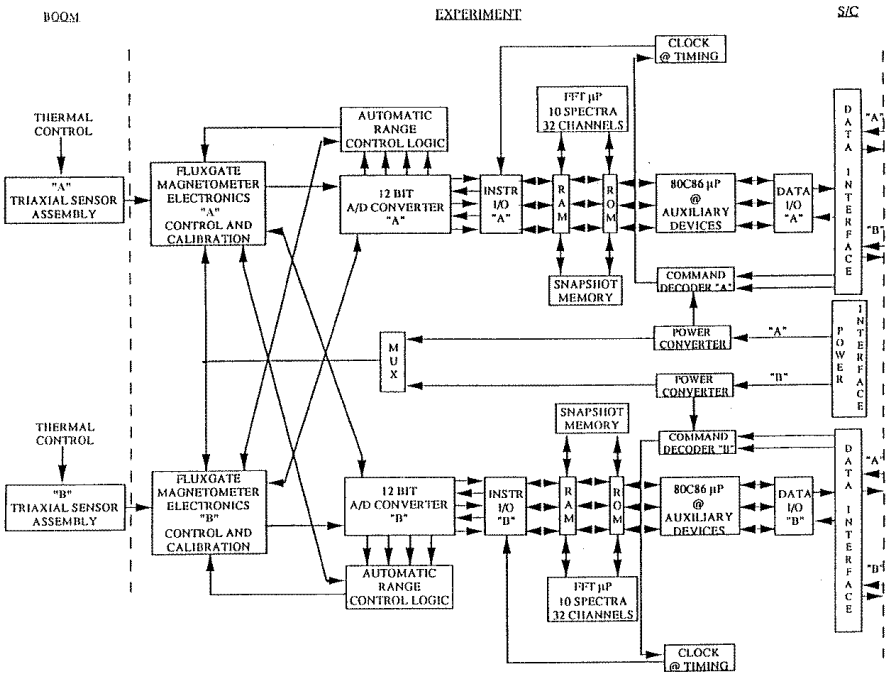

Figure 1. Block diagram of the ACE/MAG magnetic field experiment.

the role of primary or secondary sensor to either sensor triad A or B. Each magnetometer system incorporates self-resetting electronic 'fuses' which isolate the common subsystems in case of catastrophic problems.

Each sensor assembly consists of an orthogonal triaxial arrangement of ring-core fluxgate sensors plus additional elements required for autonomous thermal control. The fluxgate sensors are the latest in a series developed for weak magnetic field measurements by *Acuña* [1974] which have been used extensively in missions like Voyager, AMPTE, GIOTTO, Mars Observer, Mars Global Surveyor, etc. due to their superior performance and low power consumption. The detailed principles of the operation of fluxgate magnetometers are well known and will not be repeated here. It is sufficient to refer the reader to Figure 2 for a simplified description of their operation. (For additional information the reader is referred to *Ness* [1970], *Acuña* [1974], and *Acuña and Ness*, [1976a,b].) As shown in the figure the fluxgate sensors are driven to saturation by a 15 KHz signal derived from the DPU master clock. The sensor drive signals originate from an efficient high energy storage system which is capable of driving the ring core sensors to peak exci-

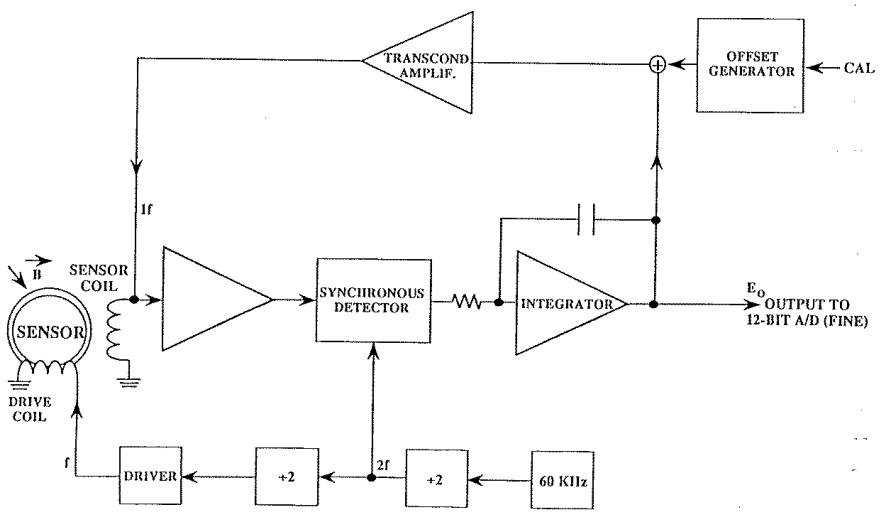

Figure 2. Schematic of standard fluxgate operation.

tations that are more than 100 times the coercive saturation force of the cores. This type of excitation eliminates from consideration many 'perming' problems which have been attributed to fluxgate sensors in the past.

In the absence of an external magnetic field, the fluxgate sensors are 'balanced' and no signal appears at the output terminals. When an external field is applied, the sensor balance is disturbed and a signal containing only even harmonics of the drive frequency appears at the output of the sensors. After amplification and filtering, this signal is applied to a synchronous detector and high gain integrating amplifier which is used to generate a current proportional to the magnitude of the applied field which is fed-back to the sensors to null the effective magnetic field as seen by it. The output of a single sensor axis is then a voltage proportional to the magnitude and direction of the ambient magnetic field with respect to the sensor axis orientation. A triaxial magnetometer is thus created when three single axis sensors are arranged in an orthogonal configuration and three sets of signal processing electronics are used to produce three output voltages proportional to the orthogonal components of the ambient magnetic field.

The noise performance of the MAG fluxgate sensors is shown in Figures 3 and 4. Total r.m.s. noise level over the 0–10 Hz band does not exceed 0.006 nT. This noise level is several orders of magnitude

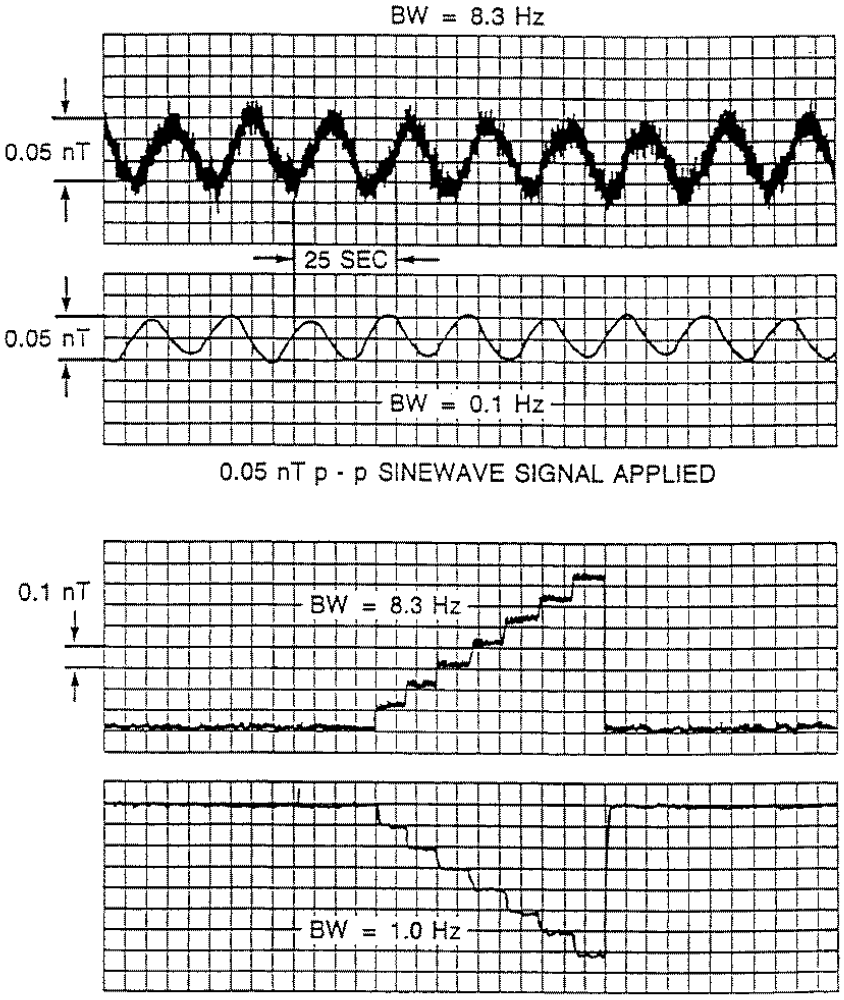

Figure 3. ACE/MAG fluxgate noise performance graphs.

below the lowest recorded levels of IMF fluctuations in this frequency range at 1 AU and is more than adequate to properly detect and identify all magnetic field phenomena of interest to ACE. Preflight tests of the spacecraft and early flight data revealed no measurable instrument- or spacecraft-associated AC signals.

The six analog signals generated by the two sensor units are digitized by the 12-bit successive approximation A/D converter. The 12-bit resolution allows the recovery of a very large dynamic range of signals

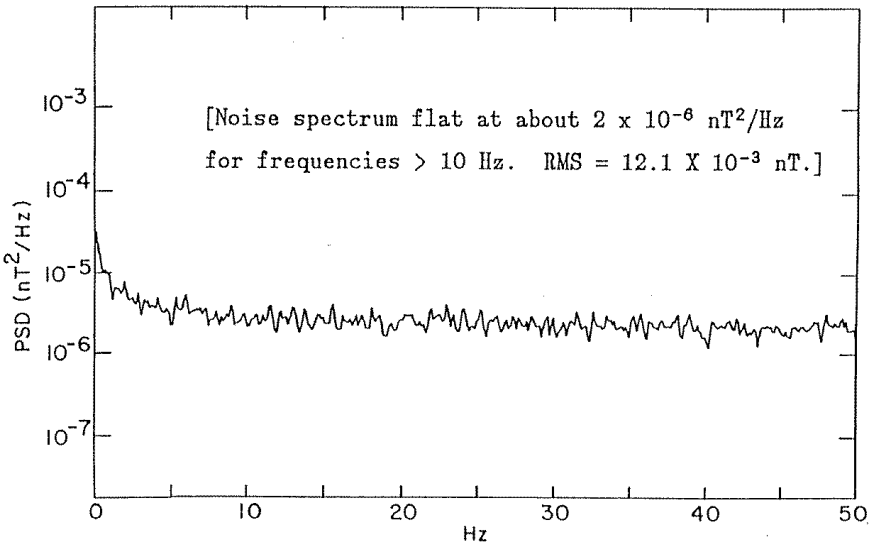

Figure 4. Noise power spectrum for MAG prototype sensor.

spanning 72 dB. To further increase the measurement dynamic range and to accommodate simplified integration and test requirements during spacecraft testing, the dynamic range of the magnetometers can be changed automatically if the magnitude of the measured signals exceeds or drops below established digital thresholds illustrated in Figure 5. In this fashion, the MAG instrumentation can cover eight orders of magnitude in magnetic field measurement capability, from 0.001 to 65,536 nT per axis.

The operation of the automatic ranging system is controlled by the microprocessor and allowed only at clearly defined times in the telemetry (once each half major frame) to avoid ambiguities in the interpretation of the data. When the digitized output of any magnetometer axis exceeds $\frac{7}{8}$th of full scale, the microprocessor generates a command to step up (increase) the magnetometer to the next, less sensitive, range. Conversely, when the output of all axes drops below $\frac{1}{8}$th of full scale, the DPU commands the appropriate sensor unit to step down (decrease) to the next most sensitive range. A 'guard band' of $\frac{1}{8}$th scale is provided to avoid the loss of measurements due to saturation until the range is updated. The factor of 4 in each range makes frequent flip-flops or oscillations between adjacent ranges unlikely. The decision to increase or decrease dynamic range is made using the basic internal sampling rate

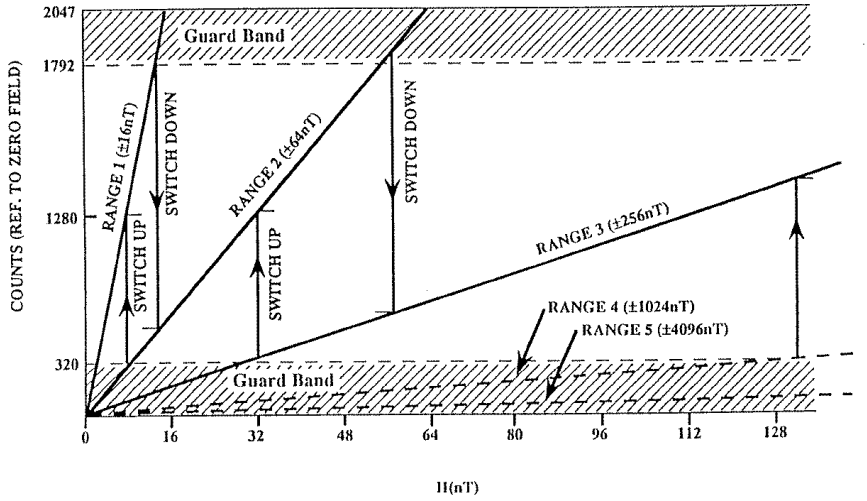

Figure 5. Range switching scheme.

of 24 vectors s^{-1}, although the periods when a range change is permitted is limited. (The Primary sensor magnetic field data is contributed to the snapshot and FFT buffers at this same rate of 24 vectors s^{-1}.) However, the MAG telemetry allocation is not sufficient to allow the transmission of all the data to the ground, so on-board data averaging, compression, and decimation must be used to reduce the 'raw' data rate to an acceptable value. These operations are described in more detail later in this paper. The DPU also controls calibration sequences which provide the necessary currents to determine the scale factor of each of the Primary and Secondary magnetometer axes for various dynamic ranges as well as the determination of zero offsets associated with electronics by implementing a 180° phase reversal of the signals processed (electronic 'flipping') [*Lepping et al.*, 1995].

4. Digital Processing Unit

The DPU, including the analog-to-digital converter, is based on the concept of a 'smart system' which performs all required operations: data manipulation and formatting, averaging, compaction and decimation, etc. The basic microprocessor used is a radiation hardened version of the popular 80C86, provided by the ISTP Project Office for development of the MFI spare, and a block diagram of the DPU architecture

is shown in Figure 1. All core operations performed by the system are carried out under the control of interrupt-driven software synchronized to the telemetry system clock, subframe and frame rates. The system design is based on a default executive and processing program which is stored and executes in Read-Only-Memory (ROM). All subsequent operations are carried out from ROM and no commands or memory loads are required to obtain valid data from the instrument after initial turn-on. All default parameter values for the system are stored in tables in ROM which, once mapped into RAM during initialization, can later be modified by ground commands to update calibrations, alignments, sampling rates, zero levels, etc. Program changes are possible in-flight through memory uploads.

The execution of the executive and auxiliary programs is monitored by hardware and software watchdog timers. The external hardware watchdog timer is normally reset by proper execution of the executive program; in the absence of a reset pulse, the watchdog timer will reset the DPU and restart the default ROM program, reloading all default parameters from ROM.

In addition to the core DPU functions described above, to better enable the study of rapid changes in the ambient magnetic field, the MAG instrument includes two additional functional elements designed specifically for this purpose: (a) a pair of 256 Kbit snapshot memory buffers and (b) an onboard FFT implemented around a TI320C10 dedicated digital signal processor and associated memory. This enables the study of the physics of the fine-scale structure of shock waves; directional discontinuities; boundary structures including those of CMEs, magnetic clouds, current sheets, and CIRs; and other transient phenomena associated with the acceleration and modulation of energetic charged particle populations, as well as the dissipation range of IMF fluctuations and other various wave modes and non-coherent fluctuations occurring regularly in the solar wind. The snapshot memory can be programmed to trigger upon the occurrence of one or more of the three classes of conditions:

1. A magnetic field magnitude jump, especially important for some kinds of shock ramp measurements.

2. A directional change (peak to peak), useful for measurements of transition regions of directional discontinuities (tangential and rotational).

3. Changes in the characteristics of field fluctuations over time, useful for some kinds of wave studies on the kinetic scale.

Two independently operating buffers, each with 256 Kbits of memory, provide the snapshot memory function of this instrument. When the selected trigger condition is satisfied, the contents of the snapshot memory are 'frozen' such that the triggering event is centrally located within the buffer and an equal interval of data both prior to and following the event is captured for later analysis. Under normal conditions, Primary sensor data sampled at the highest possible rate (24 vectors s^{-1}) is circulated through the 256 Kbit snapshot memory with cyclical overwriting once the memory is full. Thus a maximum of 7140 vector measurements can be stored in memory. This corresponds to approximately 297.5 s of data, or 4 min 57.5 s. The use of memory pointers in the DPU software allows the recovery of data acquired 148.75 s *prior* to the occurrence of the trigger (i.e., one half of the buffer). Thus, it is possible to study precursor events in high time resolution and the trigger event is located midway through the snapshot buffer record. If no trigger is observed prior to the scheduled beginning of a snapshot buffer download, the last 7140 vector measurements are sent to ground as a possible sample of high-resolution quiet-time data. The timing of the measurement is established on the ground through the use of a frame counter and comparison with the averaged data.

The FFT processor complements the snapshot memory by providing full spectral estimation capabilities in the frequency range of 0-12 Hz for Primary sensor magnetometer data. The basic FFT engine produces raw spectral estimates of the three components of the field in 256 spectral bands using 512 samples of the ambient magnetic field data (i.e. 21.3 s). In addition, the processor computes the magnitude of the magnetic field vectors in the time series being analyzed, its Fast Fourier Transform and the cross-spectral estimates associated with the three orthogonal components. In order to reduce the effects of the large signals associated with the spacecraft spin, the TI320C10 processor can be used to de-spin the spin plane components of the data prior to the computation of the FFT for these axes. Other functions included in the FFT processor are pre-whitening of input data, windowing (cosine taper and Hanning), and data compression. The latter is required to reduce the volume of raw data produced by the spectral analysis (256 spectral estimates for each element of a 3×3 spectral matrix plus a 10th spectrum, also with 256 elements, which relates to the magnitude of the IMF) to a manageable size that can be accommodated by the allocated telemetry rate for the MAG instrument. In the frequency domain, the 256 spectral estimates are compressed into 32 logarithmically spaced frequency bands of constant fractional bandwidth (or 'Q' filters). In the amplitude domain, the 12-bit data are logarithmically compressed to 7-bits plus sign using two alternate schemes: (a) a variable most-

Table II. MAG telemetry modes

Data stream	Mode 0 (BPS)	Mode 1 (BPS)	Mode 2 (BPS)
Primary[1]	108 (3 v/s)	144 (4 v/s)	216 (6 v/s)
Secondary[1]	108 (3 v/s)	72 (2 v/s)	0 (0 v/s)
FFT[2]	32 (4 comp/s)	32 (4 comp/s)	32 (4 comp/s)
Snapshot[3]	48 (4 comp/s)	48 (4 comp/s)	48 (4 comp/s)
HK and Status	8	8	8
Total	304	304	304

[1] The role of primary and secondary sensor is assigned to either sensors A or B by command.
[2] FFT vector components are 8 bits. Thirty-two bits represent 4 vector components.
[3] Snapshot vector components are 12 bits. Forty-eight bits represent 4 vector components.

significant-bit (MSB) truncation approach and (b) an algorithm based on the μ-Law commonly used in communication systems. The net result is a set of 32 full spectral matrices for the components and 32 spectral estimates for the field magnitude, transmitted to ground using 8-bit words but representing the original dynamic range of 12-bits. Further details of the FFT processor can be found in *Panetta et al.* [1991, 1992] and *Smith* [1996].

Finally, the DPU supports the distribution of 1 vector s^{-1} Primary sensor data to the NOAA Real-Time Solar Wind (RTSW) processor for immediately transmission to ground throughout the lifetime of the mission [*Zwickl et al.*, 1998]. All Status and Housekeeping bytes from each major frame of data are also sent to ground with the RTSW data to aid in data processing and interpretation. The MAG team is committed to support the processing of this data.

The three telemetry modes of the MAG instrument are illustrated in Table II. All three modes transmit a total of 304 bits s^{-1} of MAG data, status and housekeeping variables. All three modes transmit 216 bits of combined Primary and Secondary data totaling 6 vectors s^{-1}), but allocate the 216 bits differently between the two sensors according to the mode: 3 vectors s^{-1} for both Primary and Secondary sensor measurements in mode 0, 4 vectors s^{-1} for Primary sensor measurements and 2 vectors s^{-1} for Secondary sensor measurements in mode 1, and 6 vectors s^{-1} for Primary sensor measurements and 0 vectors s^{-1} for Secondary sensor measurements in mode 2. All three modes also transmit 32 bits s^{-1} of FFT data (4 compressed, 8-bit vectors s^{-1}) and require the same number of major frames of data to download the

FFT buffer. All three modes transmit 48 bits s^{-1} of snapshot data (4 non-compressed, 12-bit vectors s^{-1}) and require the same number of major frames of data to download the snapshot buffer. All three modes transmit 8 bits s^{-1} of either status or housekeeping data and 16 seconds of status and housekeeping data (1 major frame of ACE telemetry) is required to fully describe the state of the MAG instrument. The only difference between the 3 telemetry modes is the allocations for Primary and Secondary sensor data.

5. Power Converter and Thermal Control

The MAG instrumentation derives power from the 28 V regulated spacecraft bus through two redundant power converters. Only one subsystem is powered at any time. The converters are high efficiency units which operate at 50 KHz and are synchronized to the master crystal clock of the DPU to minimize interference with other experiments onboard the spacecraft. Selection of the active converter is simply accomplished by powering the desired unit.

To maintain the fluxgate sensors within their optimum operating temperature range, it is necessary to provide heater power to the boom mounted and blanketed triaxial sensor assemblies during periods of Sun occultation. (Occultation periods are not anticipated, except perhaps for a single passage through Earth's shadow on the first orbit after launch. Nevertheless, autonomous control of the MAG sensors' temperature is a feature of this magnetometer design.) Since it is extremely difficult to reduce the stray magnetic field associated with the operation of D.C. powered foil heaters to acceptable levels for MAG, a magnetic amplifier operating at 50 KHz is used to obtain automatic, proportional control of AC power supplied to the heating elements. The nominal power required to maintain the sensors at the desired temperatures in shadow is estimated to lie in the range of 0.3 to 0.5 W. No heater power should be required when the spacecraft is on station at L_1.

6. MAG Ground Data Processing

A major consideration in the design of the experiment software and operating modes is the general requirement by the ACE Project for multi-instrument, multi-user investigations. This requirement is reflected in the existence of the ACE Science Center (ASC) [*Garrard and Hammond*, 1998], the generation of preliminary Browse data by the ASC in collaboration with the instrument teams, and the deposition of

final, high-quality data in the ASC for dissemination to the community. In fulfilling this responsibility, Browse data will consist of 1 m, 5 m, 1 h, and daily averages of the IMF. The MAG experiment will provide averages of the IMF over 16 s, 4 min, and 1 hour intervals for Level-2 data products, as well as graphical representations of the data.

Time ordering of the raw telemetry (real time data transmission is interleaved with recorder playback during ground contact) is performed by the Flight Operations Team (FOT) at the GSFC along with verification of Reed-Solomon coding. The resulting time-ordered and validated Level-0 data is sent to the ASC, which reformats the data, reconstitutes MAG FFT and snapshot buffer dumps which span multiple major frames, and then forwards the resulting Level-1 data along with spacecraft position and attitude files to the Bartol Research Institute (BRI) for analysis. Data transmission to BRI will be by Internet and CD-ROM.

This same Level-1 data is processed at the ASC within one week of receipt to produce the Browse datasets [*Garrard and Hammond*, 1998]. The ASC uses routines provided by the MAG team for this purpose, but Browse data is not validated by the MAG team prior to release. Sensor offset files at the ASC will be periodically updated by the MAG team in order to maintain the highest standard of browse data possible for an automated and unverified analysis. (Likewise, the MAG team will update offset files at NOAA for use in RTSW processing [*Zwickl et al.*, 1998].)

The Level-1 MAG data, along with useful spacecraft subsystem and attitude data, is then processed at BRI to produce the final, validated and released MAG data. Level-1 data contains MAG measurements in their raw, uncalibrated, and uncorrected form. In processing the MAG data, it is necessary to evaluate the offsets for each axis of each sensor in each range for which there is data. The data is despun and rotated to physically useful coordinate systems (heliocentric (R, T, N) and Earth-centered GSE coordinates, for instance). This constitutes Level-2 data. Visualization software written in Interactive Data Language (IDL) is then used to create plots useful in scanning the data for relevant periods of interest to the investigator. These plots include both time series and color spectrograms of the data at various time resolutions. The resulting Level-2 and above data and data products, including graphs and documentation of instrument performance, are then stored on CD-ROM and transferred to the ASC for incorporation into the ASC data structure [*Garrard and Hammond*, 1998]. The estimated turn around of final MAG data products is 12 weeks.

A further, Level-3 data product is planned in cooperation with the Solar Wind Electron Proton Alpha Monitor (SWEPAM) team [*McCo-*

mas et al., 1998] wherein magnetic field and thermal particle data will be combined in a manner that is especially useful to studies of the solar wind conditions and disturbances that alter energetic particle distributions. A delivery time for this product has not yet been set, but the production of this dataset must follow the production of the Level-2 data. Snapshot memory and onboard FFT buffer data will also be included as a Level-3 data product. The data processing philosophy used for the MAG data is similar to that used for the IMP, Voyager, Mars Observer and Mars Global Surveyor data processing and will not be reviewed in detail here.

7. Summary

The ACE Magnetic Fields Experiment is a state-of-the-art, fully redundant, triaxial fluxgate magnetometer with two matching sensors flown on opposing sides of the spacecraft. Booms mounted off the $\pm Y$ solar panels place the sensors at 165 inches (= 4.19 meters) from the center of the spacecraft. The MAG instrument incorporates onboard processing of snapshot and FFT buffers to enhance the continuous 3 to 6 vectors s^{-1} measurements of the IMF by providing enhanced resolution of interplanetary transients and extension of the measured IMF fluctuation spectra to 12 Hz.

The MAG instrument will support a wide range of species-, charge- and isotope-dependent measurements that will be made by the ACE spacecraft, providing essential measurements of the *in situ* magnetic field that will permit refined analyses of the advanced particle data. MAG will also continue the long-standing tradition of studying the solar wind and interplanetary magnetic field, gaining new insights into the nature of interplanetary magnetic turbulence and serving new studies of the physics of cosmic ray propagation and acceleration.

Acknowledgements

The MAG team would like to thank P. Panetta for his efforts in reprogramming the operating system of the WIND/MFI spare for flight on ACE. We would also like to acknowledge the consideration and efforts of the managers, scientists, engineers and technicians who participated in the unofficial and voluntary, no-cost magnetics containment program. Preflight and post-launch tests indicate that magnetic contamination was adequately limited through the diligent attention and cooperation of the many ACE personnel without the imposition of a rigorous and expensive magnetics program.

References

Acuña, M. H.: 1974, IEEE Trans. Magnetics **MAG-10**, 519.

Acuña, M. H., and N. F. Ness: 1976a, in T. Gehrels (ed.), *Jupiter*, University of Arizona Press, Tucson, p. 830.

Acuña, M. H., and N. F. Ness: 1976b, *J. Geophys. Res.*, **81**, 2917.

Ambrosiano, J., W. H. Matthaeus, M. L. Goldstein and D. Plante: 1988, *J. Geophys. Res.*, **93**, 14,383.

Belcher, J. W., and L. Davis, Jr.: 1971, *J. Geophys. Res.*, **76**, 3534.

Bieber, J. W., W. H. Matthaeus, C. W. Smith, W. Wanner, M.-B. Kallenrode, and G. Wibberenz: 1994, *Astrophys. J.*, **420**, 294.

Bieber, J. W., W. Wanner, and W. H. Matthaeus: 1996, *Solar Wind 8*, Am. Inst. of Phys., p. 355.

Burlaga, J. F., R. Schwenn, and H. Rosenbauer: 1983, *Geophys. Res. Lett.*, **10**, 413.

Burlaga, L. F., F. B. McDonald, M. L. Goldstein, and A. J. Lazarus: 1993, *J. Geophys. Res.*, **98**, 1.

Burlaga, L. F.: 1995, *Interplanetary Magnetohydrodynamics*, Oxford University Press, New York.

Chiu, M. C., et al.: 1998, *Space Sci. Rev.*, this issue.

Coleman, P. J., Jr.: 1968, *Astrophys. J.*, **153**, 371.

Forman, M. A., and L. O'C. Drury: 1983, *Conf. Pap. Int. Cosmic Ray Conf.,* 18^{th}, **2**, 267.

Garrard, T. L., and J. Hammond: 1998, *Space Sci. Rev.*, this issue.

Gray, P. C., D. H. Pontius, Jr., and W. H. Matthaeus: 1996, *Geophys. Res. Lett.*, **23**, 965.

Hasselmann, K. and G. Wibberenz: 1968, *Zs. Geophys.*, **34**, 353.

Jokipii, J. R., E. H. Levy, and W. B. Hubbard: 1977, *Astrophys. J.*, **213**, 861.

Lee, M. A.: 1984, *Adv. Space Res.*, **4**, 295.

Lepping, R. P. et al.: 1995, *Space Science Reviews*, **71**, 207.

Matthaeus, W. H. and M. L. Goldstein: 1982, *J. Geophys. Res.*, **87**, 6011.

Matthaeus, W. H., M. L. Goldstein, and D. A. Roberts: 1990, *J. Geophys. Res.*, **95**, 20,673.

Matthaeus, W. H., P. C. Gray, D. H. Pontius, Jr., and J. W. Bieber: 1995, *Phys. Rev. Letters*, *75*, 2136.

McComas, D. J., S. J. Bame, P. Barker, W. C. Feldman, J. L. Phillips, P. Riley, and J. W. Griffee: 1998, *Space Sci. Rev.*, this issue.

Ness, N. F.: 1970, *Space Sci. Reviews*, **11**, 459.

Panetta, P. V., and M. H. Acuña: 1991, WIND MFI FFTP Processor Requirements Document, Rev. 10.

Panetta, P. V.: 1992, WIND MFI Flight Software Description Document, Rev. 2.

Parker, E. N.: 1963, *Interplanetary Dynamical Processes*, Wiley-Interscience, New York.

Roberts, D. A., M. L. Goldstein, L. W. Klein and W. H. Matthaeus: 1987, *J. Geophys. Res.*, **92**, 12,023.

Sanderson, T. R., R. Reinhard, P. van Nes, K.-P. Wenzel, E. J. Smith and B. T. Tsurutani: 1985, *J. Geophys. Res.*, **90**, 3973.

Simpson, J. A., et al.: 1995, *Science*, **268**, 1019.

Simpson, J. A., J. J. Connell, C. Lopate, R. B. McKibben and M. Zhang: 1995, *Geophys. Res. Lett.*, **22**, 3337.

Smith, C. W.: 1996, ACE MAG Data Formats and Algorithms, Rev. 3 (BRI document BRI-ACE-005).

Smith, C. W., and J. W. Bieber: 1993, *J. Geophys. Res.*, **98**, 9401.

Smith, C. W., and J. L. Phillips: 1997, *J. Geophys. Res.*, **102**, 249.

Tu, C.-Y., and E. Marsch: 1995, *MHD Structures, Waves and Turbulence in the Solar Wind*, Kluwer. (Reprinted from 1995: *Space Sci. Rev.*, **73** No. 1-2.)

Zank, G. P., and W. H. Matthaeus, 1992, *J. Geophys. Res.*, **97**, 17,189.
Zank, G. P., W. H. Matthaeus, and C. W. Smith: 1996, *J. Geophys. Res.*, **101**, 17,093.
Zwickl, R. D., et al.: 1998, *Space Sci. Rev.*, this issue.

Address for correspondence: J. L'Heureux, N.F. Ness and C.W. Smith, Bartol Research Institute, University of Delaware, Newark, DE 19716 (e-mail: lheureux@bartol.udel.edu, nfness@bartol.udel.edu, chuck@bartol.udel.edu), M.H. Acuña, L.F. Burlaga and J. Scheifele, Code 695, NASA/Goddard Space Flight Center, Greenbelt, MD 21043 (e-mail: macuna@gsfcmail.nasa.gov, u5jls@lepvax.gsfc.nasa.gov, u2leb@lepvax.gsfc.nasa.gov).